SISSY: an efficient and automatic algorithm for the analysis of EEG sources based on structured sparsity

Hanna Becker, Laurent Albera, Pierre Comon, Jean-Claude Nunes, Rémi Gribonval, Julien Fleureau, Philippe Guillotel, Isabelle Merlet

SISSY: an efficient and automatic algorithm for the analysis of EEG sources based on structured sparsity

H. Becker[a], L. Albera[b,c,d,*], P. Comon[e], J.-C. Nunes[b,c], R. Gribonval[d], J. Fleureau[a], P. Guillotel[a], I. Merlet[b,c]

[a] *Technicolor R&D France, F-35576 Cesson-Sévigné, France*
[b] *INSERM, U1099, Rennes, F-35000, France*
[c] *Université de Rennes 1, LTSI, Rennes, F-35000, France*
[d] *Centre INRIA Rennes-Bretagne Atlantique, Rennes, F-35042, France*
[e] *GIPSA-Lab, CNRS UMR5216, Grenoble Campus BP.46, F-38402 St Martin d'Heres Cedex*

Abstract

Over the past decades, a multitude of different brain source imaging algorithms have been developed to identify the neural generators underlying the surface electroencephalography measurements. While most of these techniques focus on determining the source positions, only a small number of recently developed algorithms provides an indication of the *spatial extent* of the distributed sources. In a recent comparison of brain source imaging approaches, the VB-SCCD algorithm has been shown to be one of the most promising algorithms among these methods. However, this technique suffers from several problems: it leads to amplitude-biased source estimates, it has difficulties in separating close sources, and it has a high computational complexity due to its implementation using second order cone programming. To overcome these problems, we propose to include an additional regulariza-

*Corresponding author: LTSI, Campus de Beaulieu, Universite de Rennes 1, 263 Avenue du General Leclerc - CS 74205 - 35042 Rennes Cedex, France, Tel: (33) – 2 23 23 50 58, E-mail: laurent.albera@univ-rennes1.fr

tion term that imposes sparsity in the original source domain and to solve the resulting optimization problem using the alternating direction method of multipliers. Furthermore, we show that the algorithm yields more robust solutions by taking into account the temporal structure of the data. We also propose a new method to automatically threshold the estimated source distribution, which permits to delineate the active brain regions. The new algorithm, called Source Imaging based on Structured Sparsity (SISSY), is analyzed by means of realistic computer simulations and is validated on the clinical data of four patients.

Keywords: EEG, sparsity, ADMM, Extended source localization

---

1. Introduction

The objective of brain source imaging consists in reconstructing the electrical activity everywhere in the brain based on surface Electroencephalography (EEG) recordings. Over the last decades, a large number of algorithms have been developed to this end; see e.g., (Baillet et al., 2001; Grech et al., 2008; Wipf and Nagarajan, 2009; Becker et al., 2015) for reviews on this topic. While most of these methods seem to be able to accurately identify the source positions, only a small number of algorithms are also suitable for determining the spatial extent of the active source regions. However, this is an important issue in some applications, such as in epilepsy. For example, for some drug-resistant patients suffering from focal epilepsy, a surgical intervention can be considered to remove the epileptogenic zone with the objective of stopping the occurence of epileptic seizures. In these cases, the precise delineation of the epileptogenic zone constitutes a crucial step of the

presurgical analysis of the patients to which brain source localization can contribute its share, e.g., by helping to guide intracranial EEG recordings. Another difficulty in brain source imaging arises in the context of propagation phenomena. When epileptic activity spreads from one brain region to another, this leads to several simultaneously active source regions with highly correlated activities. In this situation, an algorithm which can identify the positions and spatial extents of multiple source regions is desirable.

1.1. State-of-the-art

The first source imaging algorithm to take into account dependencies between adjacent grid dipoles was probably the *Low Resolution Electromagnetic Tomography (LORETA)* method (Pascual-Marqui et al., 1994). LORETA imposes spatial smoothness on the source distribution, which can be regarded as the first step towards a technique that is able to localize sources of some spatial extent. But, on the one hand, the smoothness constraint affects only the immediate neighbors of a grid dipole and is therefore too local to be effective for sources of larger extent. On the other hand, the resulting gradual changes of amplitude over space also make it difficult to delineate the source regions and to distinguish close sources.

In order to localize extended sources, (Limpiti et al., 2006) introduced the *cortical patch model*, consisting of a set of predefined, parameterized source regions. These so-called patches were then employed in a beamforming approach to identify the source regions which best described the measurements. The idea of using a fixed set of source regions was also taken up in the development of several other extended source localization approaches, including the $2q$*-th order Extended Source Multiple Signal Classification (*$2q$*-ExSo-MUSIC)*

algorithm (Birot et al., 2011), that exploits the $2q$-th order statistics of the EEG recordings with an optimization strategy based on a *Disk Algorithm (DA)*, also used for tensor-based source localization (Becker et al., 2014c). These methods achieve a good performance for the localization of a single extended source, or, in the case of tensor-based source localization, also of a small number of sources provided that they are accurately separated by the tensor decomposition step. However, localizing several highly correlated source regions remains problematic with these techniques.

A different approach for the localization of extended sources has been pursued by Ding (2009), who proposed the *Variation-Based Sparse Cortical Current Distribution (VB-SCCD)* algorithm. This source imaging method identifies piece-wise constant source distributions by imposing sparsity on the variational map, which characterizes the variations in amplitude of adjacent grid dipoles. In a recent comparison of different source imaging algorithms (Becker et al., 2014b, 2015), the VB-SCCD algorithm has been shown to yield a good performance for the localization of extended sources. In particular, it permits to simultaneously localize several highly correlated active source regions, which makes it one of the most promising approaches for the identification of multiple brain regions in the context of propagation phenomena. Nevertheless, the algorithm has some drawbacks:

- it shows difficulties in separating close sources, tending to combine them into one large source,
- the estimated source distribution may be amplitude-biased, which means that there is a systematic error on the estimated amplitudes, and

- the implementation of VB-SCCD using Second Order Cone Programming (SOCP) (Alizadeh and Goldfarb, 2001) as proposed in (Ding, 2009) leads to a high computational complexity, which practically forbids the application of the method for large numbers of time samples.

1.2. Contributions

To overcome the problems of VB-SCCD, we propose a new method, called *Source Imaging based on Structured Sparsity (SISSY)*. This algorithm includes an additional L_1-norm regularization term, which imposes sparsity on the estimated source distribution. Such an approach, also known as sparse Total Variation (sparse TV) regularization (Baldassarre et al., 2012), TV-L_1 regularization (Gramfort et al., 2013) or fused LASSO (Tibshirani and Saunders, 2005), has previously been used in image processing (Ma et al., 2008) and fMRI prediction (Baldassarre et al., 2012; Gramfort et al., 2013), where it has been shown to lead to robust solutions, but is new in the field of brain source imaging. Note though that the combination of sparsity in the original source domain and in a transformed domain that is different from the total variation has been explored in (Chang et al., 2010) for MEG source imaging. Thanks to this regularization strategy, the SISSY algorithm is able to separate even close sources and avoids amplitude-biased source estimates. In addition, we make the following contributions:

- We propose to take into account the temporal structure of the source distribution by adopting an L_{12}-norm regularization strategy as first suggested in (Ou et al., 2009), leading to more robust source estimation.

- We solve the resulting optimization problem using the Alternating Direction Method of Multipliers (ADMM) (Gabay and Mercier, 1976; Glowinski and Marrocco, 1975; Boyd et al., 2010), which considerably reduces the computational complexity compared to the SOCP algorithm employed by VB-SCCD.

- We propose a new method for selecting the regularization parameter, which does not require the estimation of the noise level.

- We develop a technique to automatically threshold the estimated source distribution based on the watershed transform (Vincent and Soille, 1991), which is a segmentation method commonly used in image processing.

Together with the proposed regularization strategy, the automatic thresholding technique makes the SISSY algorithm easy to use in clinical practice since it does not require the tedious tuning of parameters - contrary to most other currently available techniques.

To analyze the performance of the SISSY algorithm in comparison to state-of-the-art extended source localization methods, we conduct an extensive simulation study with highly realistic EEG data. Furthermore, in order to validate the proposed approach on clinical EEG data, we apply the SISSY algorithm to the EEG recordings of four epileptic patients, for which a strong hypothesis on the epileptogenic zone is available.

1.3. Organization of the paper

This paper is organized as follows: in Section 2, we introduce the underlying data model and briefly review the VB-SCCD algorithm, before presenting

the proposed SISSY method. Furthermore, we describe the simulation setup and the clinical data that are used to evaluate the SISSY algorithm. Section 3 then presents the results obtained on simulated and real data. Finally, our findings are discussed in Section 4. Section 5 concludes the paper.

Please note that parts of this work have previously been presented in (Becker et al., 2014a).

2. Methods

2.1. Data model

Mathematically, the brain electrical currents resulting from the electrochemical process of information transmission between neurons can be modeled using a grid of current dipoles, where each dipole represents a neuronal population with synchronized activity. These dipoles form the source space. As the signals that are recorded by the scalp electrodes are known to originate primarily from the pyramidal neurons in the gray matter, which are arranged in parallel with an orientation perpendicular to the surface, it is physiologically plausible to employ a source space that is composed of dipoles located on the cortical surface with an orientation perpendicular to this surface (Dale and Sereno, 1993). Assuming that the dynamics of all source dipoles are characterized by the signal matrix $\mathbf{S} \in \mathbb{R}^{D \times T}$, where T denotes the number of time samples and D is the number of source dipoles, the EEG data $\mathbf{X} \in \mathbb{R}^{N \times T}$ recorded by N sensors correspond to a linear mixture of the source signals:

$$\mathbf{X} = \mathbf{GS}. \tag{1}$$

The mixture is characterized by the lead field matrix $\mathbf{G} \in \mathbb{R}^{N \times D}$, which describes the attenuation inflicted on the dipole signals during the diffusion in the head volume conductor. Given a head model and a source space, the lead field matrix can be computed numerically using a Boundary Element Method (BEM) (Gramfort, 2009).

An extended source, also referred to as a patch, corresponds to a continguous area of cortex with highly correlated activities and can be modeled by a number of adjacent grid dipoles with synchronized signals. The indices of all grid dipoles forming the p-th extended source, $p = 1, \ldots, P$, are stored in the set Ω_p. The source space can then be divided into two sets, $\Omega_e = \cup_{p=1}^{P} \Omega_p$ and Ω_b, which contain, respectively, the indices of the grid dipoles belonging to the P extended sources and the indices of the remaining dipoles of the source space, which are assumed to emit normal background activity of the brain. The data model can then be rewritten as

$$\mathbf{X} = \sum_{k \in \Omega_e} \mathbf{g}_k \mathbf{s}_k^{\mathrm{T}} + \sum_{\ell \in \Omega_b} \mathbf{g}_\ell \mathbf{s}_\ell^{\mathrm{T}} = \mathbf{X}_e + \mathbf{X}_b \tag{2}$$

where $\mathbf{g}_k$ and $\mathbf{s}_k^{\mathrm{T}}$ correspond to the k-th column of $\mathbf{G}$ and the k-th row of $\mathbf{S}$, respectively. The matrix $\mathbf{X}_e$ characterizes the EEG data of the (epileptic) sources and $\mathbf{X}_b$ corresponds to the background activity.

2.2. Source localization and extraction

The objective of brain source imaging consists in estimating the signal matrix $\mathbf{S}$ from the data $\mathbf{X}$ for a known lead field matrix $\mathbf{G}$. As the background activity of the brain can be assumed to be of small amplitude compared to the source activity, it is then possible to identify the dipoles belonging to the set Ω_e and thereby the extended sources by thresholding the amplitudes of

the estimated signal matrix. Subsequently, we provide a short review of the classical VB-SCCD source imaging algorithm before proceeding to describe the proposed SISSY approach.

2.2.1. VB-SCCD

The VB-SCCD algorithm (Ding, 2009) assumes a piece-wise constant spatial source distribution, which is achieved by imposing sparsity on the variational map of the sources. The variational map describes the differences in amplitude between adjacent dipoles. It can be computed by applying a linear transform, characterized by the matrix $\mathbf{V}$, to the source distribution, which is equivalent to computing the total variation on the discretized cortical surface. The elements $V_{e,d}$ of $\mathbf{V}$, $e = 1, \ldots, E$, $d = 1, \ldots, D$, where E is the number of edges of the triangular grid, are given by:

$$V_{e,d} = \begin{cases} 1 & \text{if } d = d_{e,1} \\ -1 & \text{if } d = d_{e,2} \\ 0 & \text{otherwise} \end{cases} \tag{3}$$

where $d_{e,1}$ and $d_{e,2}$ are the indices of the dipoles sharing the e-th edge. This definition can also be extended to models where the source dipoles are placed at the vertices of the grid. The objective of VB-SCCD then consists in solving the following optimization problem:

$$\min_{\mathbf{s}} ||\mathbf{V}\mathbf{s}(t)||_1 \quad \text{s. t.} \quad ||\mathbf{x}(t) - \mathbf{G}\mathbf{s}(t)||_2 \leq \delta \tag{4}$$

where $\mathbf{x}(t)$ and $\mathbf{s}(t)$ correspond to the t-th columns, $t = 1, \ldots, T$, of the data and signal matrices, respectively, and δ is a regularization parameter. This parameter may be adjusted according to the acceptable upper limit

for the reconstruction error $||\mathbf{x}(t) - \mathbf{G}\mathbf{s}(t)||_2$, which depends on the noise level. In (Ding, 2009), the optimization of (4) is performed using Second Order Cone Programming (SOCP)(Alizadeh and Goldfarb, 2001; Boyd and Vandenberghe, 2004).

2.2.2. SISSY

In practice, it is reasonable to assume that only a small number of the source dipoles contribute to the signals of interest. Hence, we introduce an additional regularization term that imposes sparsity in the original source domain. Moreover, we formulate the optimization problem in a slightly different way, which enables us to use a more efficient optimization algorithm. The SISSY source estimate is thus obtained as the solution to the following optimization problem, which is equivalent to the sparse TV (Baldassarre et al., 2012) or fused LASSO (Tibshirani and Saunders, 2005) approach:

$$\min_{\mathbf{S}} \frac{1}{2}||\mathbf{X} - \mathbf{G}\mathbf{S}||_{\mathrm{F}}^2 + \lambda(||\mathbf{V}\mathbf{S}||_1 + \alpha||\mathbf{S}||_1). \tag{5}$$

The regularization parameter λ balances between the reconstruction error and the constraint, corresponding to the first and second term in (5), respectively, and can be seen as an equivalent of the regularization parameter δ employed by VB-SCCD. The SISSY solution also depends on the additional regularization parameter α. Varying this parameter permits us to adjust the size of the reconstructed source region (the larger α, the smaller the estimated source) and prevents the estimated signal vector from featuring a large amplitude bias, which is a problem that frequently arises using the VB-SCCD algorithm. For $\alpha = 0$, the SISSY algorithm is technically equivalent to VB-SCCD, whereas setting $\alpha = 1$ leads to very focal source estimates

without amplitude bias. While this parameter could also be chosen greater than 1, reasonable results are obtained when α lies within the interval $[0, 1]$. The regularization parameter λ is generally adjusted based on an estimate of the noise level. However, since there is no direct relation between λ and the noise level - contrary to the regularization parameter δ in (4), which directly corresponds to the upper limit of the reconstruction error - different values of λ need to be tested in order to obtain a reconstruction error that lies within a given interval. Here, we also propose an alternative approach for choosing the regularization parameter λ, which is based on the following observations: in order to impose sparsity on the sources and the variational map, we would ideally employ an L_0-norm regularization. However, as it is mathematically not possible to solve the L_0-norm optimization problem in a reasonable amount of time (NP-hard problem), we resort to L_1-norm regularization instead, for which efficient solvers exist. Now, comparing the L_0-norm and L_1-norm regularization terms of the solutions obtained for several different values of λ, we note that up to a certain value, increasing λ, i.e., increasing the impact of the regularization term, effectively leads to a decrease of both the L_1-norm and the L_0-norm of the regularization terms. Yet above this threshold value, only the L_1-norm keeps decreasing whereas the L_0-norm increases again. Our idea is to select, among the tested values, the regularization parameter that corresponds to this threshold, thus heuristically minimizing the L_0-norm regularization term $||\mathbf{VS}||_0 + \alpha||\mathbf{S}||_0$.

Exploitation of temporal structure. The SISSY algorithm as described in the previous section considers each time sample independently and thus does not take into account the temporal structure of the data. However, it can be

expected that if only a short time interval is considered (corresponding, e.g., to the duration of an interictal epileptic spike), the active source regions stay the same. This hypothesis can be enforced by replacing the L_1-norm in (5) by the $L_{1,2}$-norm, which is defined as follows: $||\mathbf{S}||_{1,2} = \sum_{d=1}^{D} \sum_{t=1}^{T} S_{d,t}^2$. The $L_{1,2}$-norm promotes a row-sparse structure with a small number of non-zero rows corresponding to active dipoles and many zero rows for inactive dipoles. This permits to obtain more robust source estimates. The resulting source localization approach is subsequently called $L_{1,2}$-SISSY.

Optimization using ADMM. The optimization problems of both algorithms, SISSY and $L_{1,2}$-SISSY, can be rewritten in a generalized, constrained optimization framework with latent variables $\mathbf{Y}$ and $\mathbf{Z}$:

$$\begin{aligned} \min_{\mathbf{S}} \frac{1}{2}||\mathbf{X} - \mathbf{GS}||_{\mathrm{F}}^2 + \lambda(f(\mathbf{Y}) + \alpha f(\mathbf{Z})) \\ \text{s. t.} \quad \mathbf{Y} = \mathbf{VS}, \quad \mathbf{Z} = \mathbf{S}. \end{aligned} \tag{6}$$

Here, f represents the regularization function that is either the L_1-norm (for SISSY) or the $L_{1,2}$-norm (for $L_{1,2}$-SISSY). Problem (6) can be solved using ADMM (Gabay and Mercier, 1976; Glowinski and Marrocco, 1975; Boyd et al., 2010), which is a simple and efficient algorithm for constrained convex optimization. It is based on the idea of alternatingly updating the variables $\mathbf{S} \in \mathbb{R}^{D \times T}$, $\mathbf{Y} \in \mathbb{R}^{P \times T}$, and $\mathbf{Z} \in \mathbb{R}^{D \times T}$ in the augmented Lagrangian of (6), as well as computing alternating updates of the scaled Lagrangian multipliers $\mathbf{U} \in \mathbb{R}^{P \times T}$ and $\mathbf{W} \in \mathbb{R}^{D \times T}$. After initialization (for example, by setting all variables to zero), at the k-th iteration, the following update rules can be

derived:

$$
\begin{aligned}
\mathbf{S}^{(k+1)} &= \mathbf{P}^{-1}\left[\mathbf{G}^{\mathrm{T}}\mathbf{X} + \rho\mathbf{V}^{\mathrm{T}}(\mathbf{Y}^{(k)} - \mathbf{U}^{(k)}) + \rho(\mathbf{Z}^{(k)} - \mathbf{W}^{(k)})\right] \\
&\text{with} \quad \mathbf{P} = \mathbf{G}^{\mathrm{T}}\mathbf{G} + \rho(\mathbf{V}^{\mathrm{T}}\mathbf{V} + \mathbf{I}) \\
\mathbf{Y}^{(k+1)} &= \mathrm{prox}_{f,\lambda/\rho}\left(\mathbf{V}\mathbf{S}^{(k+1)} + \mathbf{U}^{(k)}\right) \\
\mathbf{Z}^{(k+1)} &= \mathrm{prox}_{f,\lambda\alpha/\rho}\left(\mathbf{S}^{(k+1)} + \mathbf{W}^{(k)}\right) \\
\mathbf{U}^{(k+1)} &= \mathbf{U}^{(k)} + \mathbf{V}\mathbf{S}^{(k+1)} - \mathbf{Y}^{(k+1)} \\
\mathbf{W}^{(k+1)} &= \mathbf{W}^{(k)} + \mathbf{S}^{(k+1)} - \mathbf{Z}^{(k+1)}
\end{aligned}
$$

where $\rho > 0$ denotes the penalty parameter introduced in the augmented Lagrangian (see (Boyd et al., 2010); here we set $\rho = 1$). Please note that in practice, the computation of the inverse of the large matrix $\mathbf{P} \in \mathbb{R}^{D\times D}$ should be avoided, for example, by resorting to an inversion lemma and matrix decompositions (such as the QR-decomposition) which can be computed efficiently. The updates of $\mathbf{Y}$ and $\mathbf{Z}$ are formulated using the proximity operator, originally introduced in (Moreau, 1962), which is given by:

$$
\mathrm{prox}_{f,\beta}(\mathbf{Y}) = \arg\min_{\mathbf{X}} \frac{1}{2}||\mathbf{Y} - \mathbf{X}||_{\mathrm{F}}^2 + \beta f(\mathbf{X}). \tag{7}
$$

Solutions to (7) for f corresponding to the L_1-norm (known as soft-thresholding) or the $L_{1,2}$-norm of $\mathbf{X}$ can be found in (Combettes and Pesquet, 2008; Gramfort et al., 2012). The algorithm is stopped after convergence or a maximal number of iterations is reached.

2.2.3. Automatic thresholding

To delineate the source regions from the estimated source distributions, the dipole amplitudes need to be thresholded. Depending on the selected

threshold, the source estimates can thus vary considerably in size and form. To overcome this problem, we propose an Automatic Thresholding (AT) method, applied in a second step after the estimation of the signal matrix, that leads to an objective delineation of the source regions based on the gradient of the estimated source distribution. The proposed method is based on the watershed transform (Vincent and Soille, 1991), which is commonly used for image segmentation, and consists of three steps.

Step 1:. The triangular cortical surface can be viewed as a graph, where the triangles (grid dipoles) correspond to the nodes and the edges between triangles correspond to the edges of the graph. Each edge is assigned an amplitude that is equal to the absolute value of the corresponding element of the variational map. The first step of the AT method then consists in applying the watershed transform on the edges of the graph. The watershed transform thus permits to segment the source space into groups of adjacent dipoles with similar amplitudes. The border between adjacent groups is characterized by an increased gradient between adjacent dipoles. This leads to a first parcellization of the source space.

Step 2:. As the number of source regions in this first parcellization is still relatively high (several dozens), the identified source regions are subsequently merged until only source regions that correspond to a local amplitude maximum or minimum remain. To this end, the following procedure is employed:

1. Identify the two adjacent source regions with the smallest difference in average amplitude.
2. Merge the regions unless this would reduce the number of local ampli-

tude maxima/minima (e.g., two regions are not allowed to merge if this would lead to two distinct local maxima to become adjacent or if one region is a local maximum and the other region corresponds to a local minimum).

3. Repeat 1. and 2. until there remains no pair of adjacent regions that are allowed to be merged.

Step 3:. After identifying all regions corresponding to local amplitude extrema, we finally identify the regions that contribute to the EEG recordings in a significant way by thresholding the average amplitudes of all regions by a suitable value (e.g., 10 % of the maximum amplitude).

2.3. Simulations

To compare the performance of SISSY to state-of-the-art methods such as STWV-DA, 4-ExSo-MUSIC, and cortical LORETA (cLORETA) (Wagner et al., 1996), we conduct an extensive simulation study with realistic EEG data in the context of interictal epileptic extended source localization.

2.3.1. Data generation

We generate physiologically plausible EEG data according to the forward model described in section 2 for $N = 91$ electrodes using a realistic head model with three compartments that represent the brain, the skull, and the scalp. The source space consists of $D = 19626$ dipoles corresponding to the triangles of the cortical surface mesh with orientations perpendicular to the cortical surface. A BEM method (ASA, ANT, Enschede, Netherlands) is used to compute the lead field matrix. For simplicity, we use the same volume conductor and source space for the forward and the inverse problem.

Please note that in practice, modeling errors additionally impact the source localization results, but this effect is common to all algorithms and is not studied in this paper.

To model extended sources, we consider a certain number of patches on the left hemisphere. If not stated otherwise, the patches are composed of 100 adjacent grid dipoles, corresponding to an area of approximately 5 cm^2 of active cortex as required in order to obtain a signal of sufficient amplitude to be measurable on the scalp according to previous studies (Mikuni et al., 1997; Oishi et al., 2002; Shigeto et al., 2002; Gavaret et al., 2006; Tao et al., 2005; Merlet and Gotman, 1999; Ebersole, 1997)The shapes of these patches have been chosen to follow the sulci and gyri of the cortex and to be different from the circular shape that is used in the dictionary of potential distributed sources underlying the STWV-DA and 4-ExSo-MUSIC algorithms. To generate the source dynamics, we use an epileptic spike signal comprising $T = 200$ time samples (at 256 Hz sampling frequency) that was segmented from stereotactic EEG (SEEG) recordings of a patient suffering from epilepsy. Different realizations of this signal, one for each patch dipole, are then created by introducing small variations in amplitude and delay. More precisely, a variation $\tilde{s}(t)$ of the template signal $s(t)$ is generated as $\tilde{s}(t) = as(t + \tau)$ where a is randomly drawn from the log-normal distribution $\ln(N(0, 0.01))$ and τ is randomly drawn from the normal distribution $N(0, 4)$. For multipatch scenarios, we assume that patches are activated due to a propagation of the epileptic activity of the first patch. Therefore, we use the same signals for the dipoles of these secondary patches, but introduce a delay of 4 to 24 ms depending on the distance to the first patch. All source

dipoles that do not belong to a patch are attributed zero-mean Gaussian background activity with an amplitude that is adjusted to the amplitude of the SEEG signals between epileptic spikes, thus leading to realistic Signal to Noise Ratios (SNR) such that $||\mathbf{GS}||_{\mathrm{F}}^2/||\mathbf{N}||_{\mathrm{F}}^2 \approx 1$.

2.3.2. Source imaging

The EEG data are spatially prewhitened before applying the source localization algorithms. To this end, an estimate of the noise covariance matrix is employed, which is derived based on the variance and the spatial correlation structure of the background activity. To adjust the regularization parameter λ, for single patch scenarios, we employ the new selection strategy presented in Section 2.2.2 because the noise level based selection strategy does not work for small patches, where it is very difficult to find a parameter λ that yields a reconstruction error in the given interval. For multipatch scenarios, we employ the noise level based regularization strategy because the proposed strategy based on the L_0-norm tends to yield too sparse source estimates in some cases, eliminating part of the estimated patches. If not stated otherwise, we consider two fixed values for the second regularization parameter, $\alpha = 0$, leading to solutions equivalent to VB-SCCD, and $\alpha = 0.07$ because we found that this leads to reasonable results for the considered scenarios.

For SISSY and cLORETA, which provide one source estimate per time sample, we determine the active patches by thresholding the source estimates at the data sample of maximal power, corresponding to the maximum of the epileptic spike. For each identified source region, comprised of adjacent dipoles, we then compute the average of the time signals of all involved source dipoles in order to obtain one estimated time signal per patch. For 4-ExSo-

MUSIC, an estimate of the patch signals is computed as $\hat{\mathbf{S}} = \mathbf{H}^{+}\mathbf{X}$. Here, $\mathbf{H}^{+}$ denotes the pseudoinverse of the spatial mixing matrix $\mathbf{H} \in \mathbb{R}^{N \times R}$ whose r-th column corresponds to the sum of the lead field vectors associated to the dipoles belonging to the r-th estimated patch. No further processing is necessary in case of STWV-DA, as this algorithm already provides a time signal for each estimated extended source at its output.

2.3.3. Evaluation criteria

The performance of the source imaging results is assessed using the Dipole Localization Error (DLE) (Yao and Dewald, 2005), which characterizes the similarity between the original and the estimated source configurations. If $\mathcal{I}$ and $\hat{\mathcal{I}}$ denote the original and estimated sets of indices of all dipoles belonging to an active patch, Q and $\hat{Q}$ are the numbers of original and estimated active dipoles, and $\mathbf{r}_k$ denotes the position of the k-th source dipole, then the DLE is defined as:

$$\mathrm{DLE} = \frac{1}{2Q} \sum_{k \in \mathcal{I}} \min_{\ell \in \hat{\mathcal{I}}} ||\mathbf{r}_k - \mathbf{r}_\ell|| + \frac{1}{2\hat{Q}} \sum_{\ell \in \hat{\mathcal{I}}} \min_{k \in \mathcal{I}} ||\mathbf{r}_k - \mathbf{r}_\ell||.$$

The quality of the extracted signals is evaluated by calculating the correlation coefficients between the estimated patch signal and the averaged signal of all dipoles belonging to a patch. We then compute the mean of the correlation coefficients for all patches.

2.4. Clinical data

The feasibility of SISSY was tested on 32-channel data recorded in four patients with epilepsy. The sampling rate was 1000 Hz in 3 patients and 256 Hz in one patient. Thus for our analysis, data were all subsampled

to 250 Hz. Patient-specific head models were derived for three patients by segmenting the surfaces of the brain, the skull, and the scalp from MRIs of the patients. For these patients, the source space was composed of about 15000 dipoles corresponding to the vertices of the cortical surface mesh. The lead field matrices were computed using the BEM method implemented in OpenMEEG (Gramfort et al., 2010; Kybic et al., 2005). For one patient (number 4), the MRI could only be partially segmented, but since there was no lesion, we used the template head model that was employed for the simulations. For each patient, spikes were categorized according to their voltage distribution and averaged. For patient 1, we analyzed the average of 5 spikes that are maximal on electrode T4, for patient 2, we considered the average of 6 spikes maximal on electrode FFT9, for patient 3, we analyzed the average of 6 spikes maximal on electrode PPOz, and for patient 4, we considered the average of 7 spikes maximal on electrode FT10. Patient 3 had already undergone a previous surgery where part of the left occipital cortex had been removed, but still was not seizure-free. Intracranial SEEG recordings were acquired for all patients as part of the presurgical evaluation. The SEEG data were analyzed by an expert, resulting in strong hypotheses on the brain regions involved in the interictal epileptic activity. These data are summarized in Figure 1.

The proposed method was then applied to the epileptic spikes of the four patients and the results were compared to those of cLORETA, STWV-DA, and 4-ExSo-MUSIC. For SISSY, the regularization parameter was chosen using the proposed criterion based on the L_0-norm and the localized brain regions were delineated using AT whereas for cLORETA, STWV-DA, and 4-

	Age (age at onset)	Handi-ness	Type of seizures	# of depth electr.	MRI	Intracerebral interictal activity	Conclusion from depth EEG recordings (interictal activity)
1	29 (11)	R	Right temporal seizures with independent temporo-parietal abnormalities	12 (R) 2(L) (not shown)	Normal	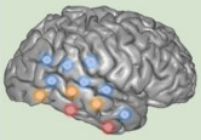	Right anterior or median inferior temporal gyrus, with diffusion to median and posterior aspects of the inferior and middle temporal gyri.
2	38 (12)	R	Left temporal seizures with involvement of insula and/or operculum	12 (L)	Signal abnormality in the left temporal pole, and basal insula	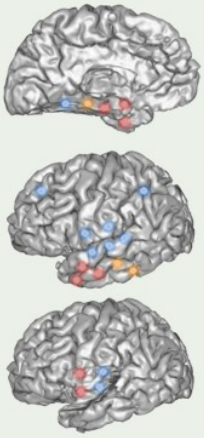	Large area in the left temporal lobe and insula including : 1.mesial temporal regions (hippocampus, entorhinal cortex, parahippocampal gyrus 2.basal aspect of the temporal pole (mesial and lateral), the anterior middle and inferior temporal gyrus 3. basal and superior anterior insula
3	30 (3)	R	Left parieto-occipital seizures	6 (L)	Left Focal Cortical Dysplasia in the mesial parieto-occipital region operated in 2002	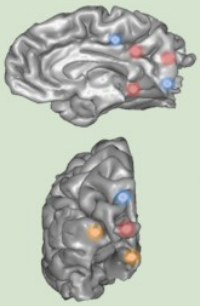	Left posterior cingulate gyrus, left cuneus, precuneus and inferior parietal region (remaining after previous surgery)
4	38 (24)	R	Right temporal sizures	13(R) 1(L)	Right anterior temporal atrophy	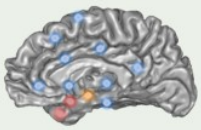	1.Right temporal pole , and anterior aspect of the middle temporal gyrus 2.Right mesial temporal pole, amygdala, and basal insula 3.Inferior temporal gyrus

Figure 1: Summary of the SEEG analyses of the four patients. Note that the SEEG results concerning the interictal epileptic activity reported here are those that correspond best to the topography of spikes recorded during the scalp EEG session. The findings of the SEEG are illustrated for each patient on the patient-specific mesh (including for patient 4, where the cortical surface could be segmented from the MRI, but not the complete head model) with a lateral, semi-lateral (showing the insula) or mesial view depending on the patient. The red points mark the primary interictal activity, the orange points indicate propagated interictal activity, and the blue points mark the regions that have been analyzed by SEEG, but do not show any significant interictal activity.

ExSo-MUSIC, the active source regions were selected based on the goodness-of-fit (GOF, see, e.g., (Becker et al., 2014c)). Finally, the source localization results of the different tested algorithms were compared to the findings of the SEEG analysis.

3. Results

3.1. Single-patch scenarios

In order to analyze the influence of the regularization parameter α on the performance of the SISSY algorithm, we consider 5 patches at different positions and of varying sizes from 10 grid dipoles (about 0.5 cm^2) to 300 grid dipoles (about 15 cm^2). The patches are located on the inferior parietal gyrus (InfPa), the superior frontal gyrus (SupFr), the superior occipital gyrus (SupOcc), the basal temporal gyrus (BasTe) and the mid-temporal gyrus (MidTe). The DLE values obtained for these patches are shown in Figure 2 for six different values of the parameter α (0, 0.07, 0.1, 0.2, 0.5, and 1) and for six different patch sizes (10, 25, 50, 100, 200, and 300 patch dipoles). To improve the resolution of the small DLE values, we have limited the color scale to a maximum DLE of 10 mm, which means that DLE values exceeding this threshold are represented as 10 mm in the figure. In any case, the source reconstructions corresponding to DLE values of 10 mm and more can be considered to be inacceptable such that the exact DLE value is of no practical importance.

As Figure 2 shows, for small patch sizes, the DLE values are very high. More particularly, for the superficial patches InfPa, SupFr, and SupOcc, a minimal patch size of 50 dipoles, corresponding to about 2.5 cm^2 of cortex,

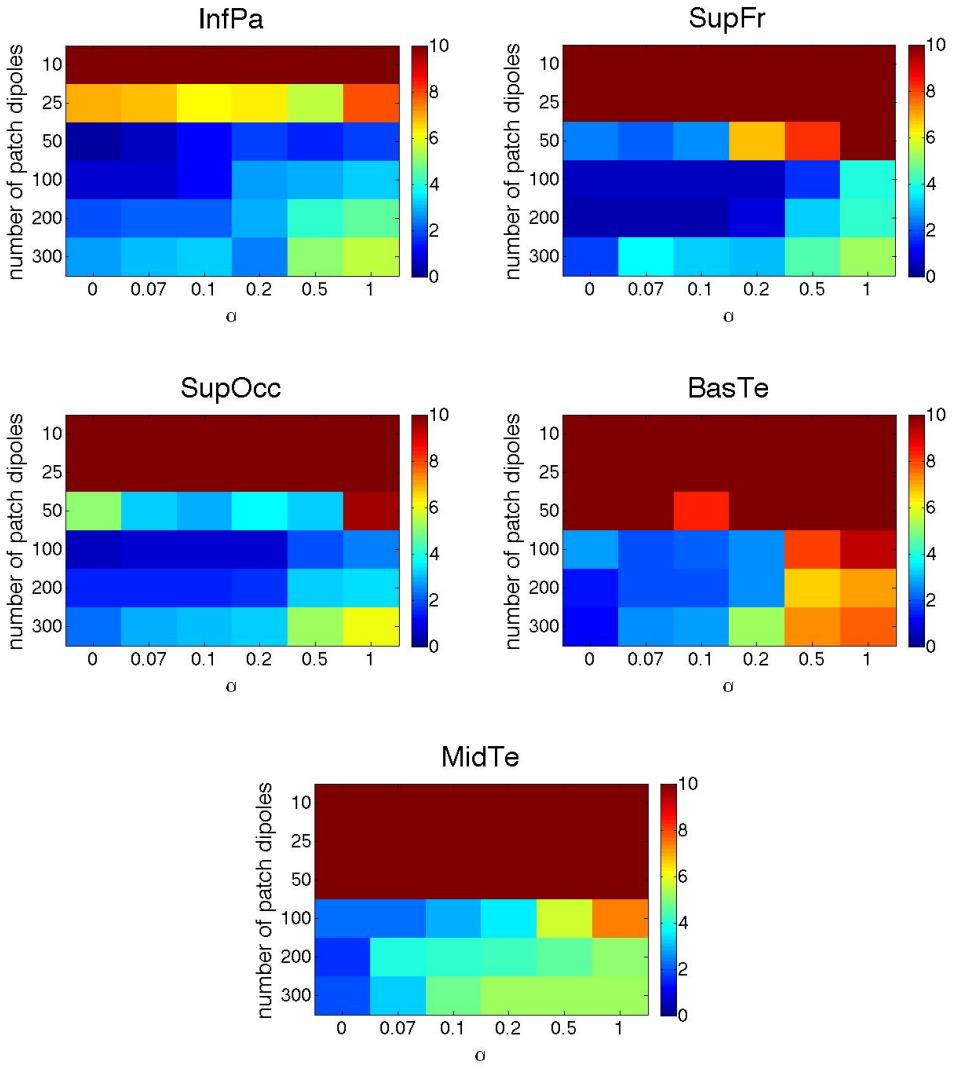

Figure 2: Dipole Localization Error (DLE) coded in color (the smaller (blue) the better) for different patch positions depending on the patch size and the regularization parameter α. Note that the upper limit of the DLE has been fixed to 10 mm, meaning that DLE values higher than this threshold have been replaced by 10 mm.

is required to yield accurate localization results whereas for the lateral patch MidTe and the deeper patch BasTe, the patches need to be composed of at least 100 dipoles, corresponding to about 5 cm^2 of cortex. Above the minimal size threshold, the DLE slightly increases with augmenting patch size.

Concerning the influence of the regularization parameter, while the source estimates change only slightly with small variations of the parameter α, the DLE values generally increase with increasing α, such that the best results are achieved for $\alpha = 0$ or $\alpha = 0.07$. Therefore, we consider only the latter two values in the following.

3.2. Multi-patch scenarios

In this section, we consider 4 different scenarios:

- Scenario 1: three patches with medium to large distances, located on the superior frontal (SupFr), inferior frontal (InfFr), and superior occipital (SupOcc) gyrus,
- Scenario 2: three close patches, located on the mid temporal (MidTe), occipital temporal (OccTe), and inferior parietal (InfPa) gyrus,
- Scenario 3: four close patches: OccTe, MidTe, SupOcc, InfPa,
- Scenario 4: five close patches: OccTe, MidTe, InfPa, SupTe (superior temporal gyrus), and SupOcc.

First of all, we illustrate in Figure 3 the different steps of the AT procedure for the second scenario (patches MidTe, OccTe, and InfPa). In the first step, the watershed transform permits to identify a large number of regions (27 in this example) such that the amplitudes of the dipoles belonging to each region

are approximately identical. In the second step, these regions are merged until only regions that are local maxima or minima remain (in this example, this leads to 9 regions). Finally, the amplidutes of the remaining regions are thresholded in a third step, yielding a source configuration with only three regions that correspond to the patches in the original source distribution.

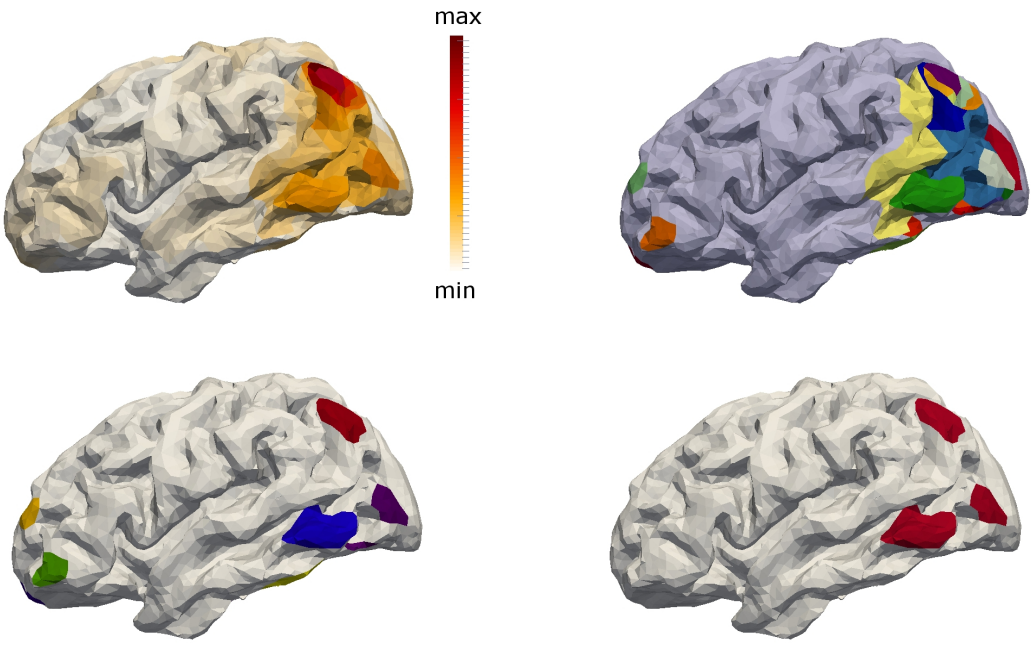

Figure 3: Illustration of the automatic thresholding approach: original source distribution (top left), regions identified by the watershed transform in step 1 of AT (top right), remaining regions after region fusion in step 2 of AT (bottom left), and final result after thresholding of region amplitudes in step 3 of AT (bottom right).

Next, we compare the performance of different SISSY variants for the four considered scenarios to the performance of cLORETA, STWV-DA, and 4-ExSo-MUSIC. Figure 4 shows boxplots of the DLE values obtained over 50 different realizations for each scenario. It can be observed that the DLEs of

SISSY for $\alpha = 0.07$ are always smaller than those of cLORETA, STWV-DA, and 4-ExSo-MUSIC for all considered scenarios. For $\alpha = 0$, this is also the case for scenarios 1 and 4, but not for scenarios 2 and 3. Comparing the results of SISSY for different values of the regularization parameter α, we note that for $\alpha = 0.07$, i.e., with additional regularization in the source domain, SISSY yields smaller DLEs than for $\alpha = 0$. Furthermore, $L_{1,2}$-SISSY leads to smaller DLE than SISSY, in particular for $\alpha = 0.07$, where it also reduces the variance of the observed DLE values, but for $\alpha = 0$, the difference between the DLE of $L_{1,2}$-SISSY and SISSY is rather small. To get a better insight on the performance of the different methods, we also show in Figures 5 to 8 the source distributions that are estimated by the tested source imaging algorithms as well as the thresholded sources for the different SISSY variants. These figures show that all methods except cLORETA yield good estimates of the three distant patches in scenario 1 (even though 4-ExSo-MUSIC overestimates the size of the patch SupOcc). However, for the three other scenarios that involve several close patches, STWV-DA and 4-ExSo-MUSIC do not work well, failing to recover all patches, leading to bad estimates of the shapes of the correctly identified patches and including spurious sources for scenarios 3 and 4. For scenarios 2 and 3, the source distributions estimated by cLORETA show high amplitudes at the positions of the patches, yet they make it difficult to infer the patch size and shape and also include high amplitudes at a position that does not correspond to a patch of the original source configuration. For scenario 4 as for scenario 1, cLORETA fails completely to recover a correct solution. Concerning the performance of the different variants of SISSY, we observe that for $\alpha = 0$,

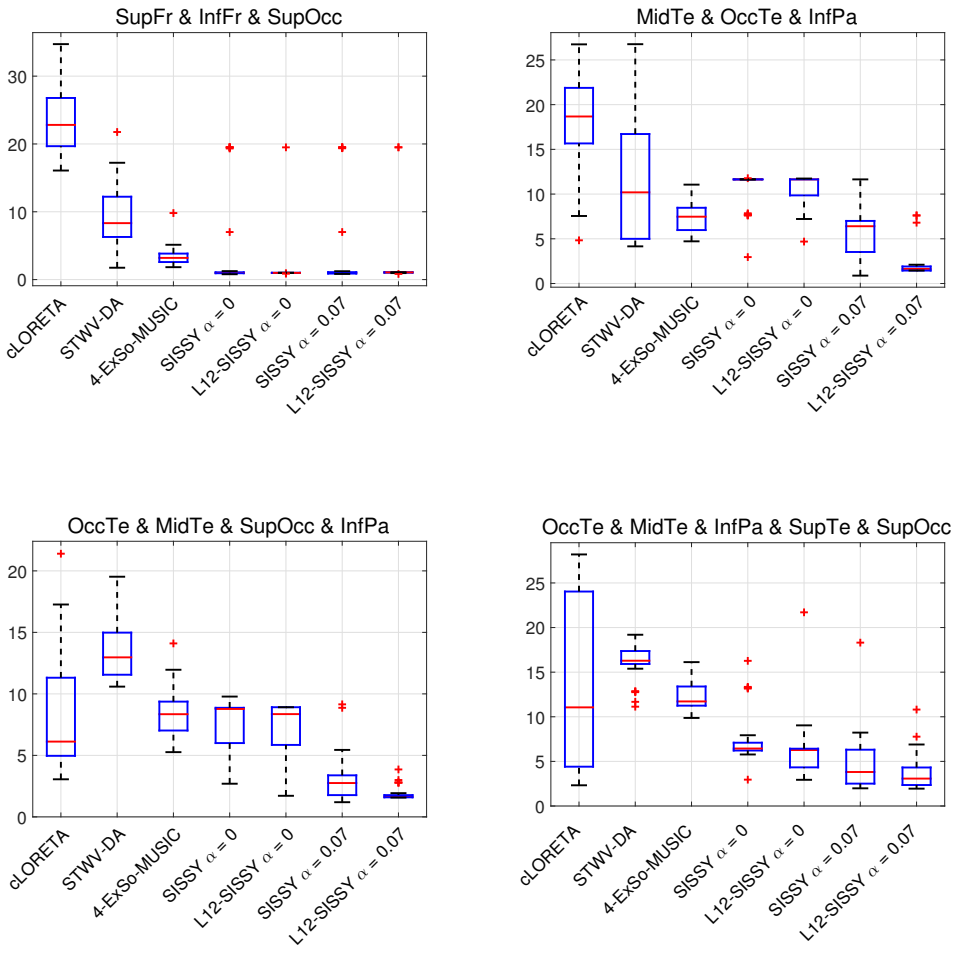

Figure 4: Boxplots of Dipole Localization Error (DLE) results (the lower the better) of the tested source imaging algorithms for 4 different multi-patch scenarios and 50 realizations with different signals and background activity.

the algorithm shows some difficulties in recovering all patches. More particularly, the patches MidTe and OccTe, which are located in the temporal lobe and thus have lower amplitudes at the surface than the patches InfPa and SupOcc, are missing in the estimated source distributions for scenarios 2 and 3, whereas for scenario 4, the algorithm does not separate the five active patches. Expoiting the temporal structure in $L_{1,2}$-SISSY ($\alpha = 0$), one obtains somewhat improved source estimates, but the performance is enhanced more by considering the additional regularization term ($\alpha = 0.07$). The best results are achieved for $L_{1,2}$-SISSY with $\alpha = 0.07$. In this case, the algorithm correctly recovers all patches for all four considered scenarios.

Furthermore, in Fig. 6, we also show the estimated patch signals for SISSY in comparison to the original, simulated patch dynamics for scenario 2. It can be seen that SISSY yields good estimates of the source dynamics. In particular, for L12-SISSY with $\alpha = 0.07$, which has separated all three patches, the estimated patch signals show that patches OccTe and MidTe are activated prior to the patch SupOcc. However, due to the small distance and small delay between the signals of patches MidTe and OccTe, these patches appear to be simultaneously activated in the inverse solution and the small time delay cannot be resolved in the source estimation.

Quantitatively, the performance of the different algorithms in estimating the source time courses is evaluated using the signal correlation coefficients, which are given in Table 1. The signal correlation coefficients achieved by SISSY are clearly higher than those for all other methods. Moreover, the correlation between the original signals and those extracted by $L_{1,2}$-SISSY is generally higher than for the signals estimated by SISSY. The highest

correlation coefficients are achieved by $L_{1,2}$-SISSY for $\alpha = 0.07$.

signal correlation (%)	scenario 1	scenario 2	scenario 3	scenario 4
cLORETA	35.6	25.9	71.2	43.2
STWV-DA	67.1	84.1	86.3	86.8
4-ExSo-MUSIC	82.7	70.2	70.1	62.9
L1-SISSY $\alpha = 0$	91.5	85.1	90.1	90.2
$L_{1,2}$-SISSY $\alpha = 0$	97.2	89.3	93.3	91.3
L1-SISSY $\alpha = 0.07$	93.1	89.9	90.1	90.4
$L_{1,2}$-SISSY $\alpha = 0.07$	97.6	96.8	96.9	95.7

Table 1: Average signal correlation coefficient between original patch signals and estimated patch signals.

Finally, to give the reader an idea of the computational complexity of the different considered source imaging methods, we indicate the CPU times of the algorithms in Table 2. For comparison, we also provide the CPU time of the original VB-SCCD algorithm. The algorithms are implemented in Matlab2012a on a computer with a 3.2 GHz Intel Core i5 processor and 8GB of RAM. Note, however, that parts of 4-ExSo-MUSIC are implemented in C, such that its CPU time is not directly comparable to that of the other methods. For algorithms that can work on a single time sample, such as cLORETA, SISSY, and VB-SCCD, we indicate the CPU time if the algorithm is applied to one time sample, whereas for STWV-DA, 4-ExSo-MUSIC, and $L_{1,2}$-SISSY, all 200 time samples are processed by the algorithms. The smallest CPU time is required by cLORETA, followed by SISSY, which takes about 5 s and which is much faster than VB-SCCD by a factor of about 20.

Taking into account all time samples, running $L_{1,2}$-SISSY takes about 2 minutes, whereas executing STWV-DA takes 20 s longer, making it the slowest of all tested algorithms.

	algorithm	CPU time in seconds
algorithms working on a time sample-by-sample basis	cLORETA	0.6
	L1-SISSY $\alpha = 0$	4.9
	L1-SISSY $\alpha = 0.07$	4.9
	VB-SCCD	97.1
algorithms taking into account all time samples	STWV-DA	141.0
	4-ExSo-MUSIC	59.4
	$L_{1,2}$-SISSY $\alpha = 0$	119.1
	$L_{1,2}$-SISSY $\alpha = 0.07$	117.9

Table 2: Mean CPU time (averaged over the 6 scenarios)

3.3. Patch separation

In this section, we aim at analyzing more precisely the resolution of the considered source imaging algorithms, i.e., the capability to separate two patches depending on their distance. To this end, we consider 6 patches of similar form (cf. Fig. 9) and 4 different distances. As the separation of the patches does not only depend on their distance, but also on their position, we study several scenarios for each distance:

- distance 1 (≈ 1.8 cm): P1 & P2, P2 & P3, P3 & P4, P4 & P5, and P5 & P6;
- distance 2 (≈ 3.4 cm): P1 & P3, P2 & P4, P3 & P5, and P4 & P6;

- distance 3 (≈ 5.2 cm): P1 & P4, P2 & P5, and P3 & P6;
- distance 4 (≈ 6.7 cm): P1 & P5 and P2 & P6.

We consider two patches to be separated if the estimated source configuration contains two patches such that one estimated patch overlaps with the first original patch and the other estimated patch overlaps with the second original patch. By analyzing 10 different realizations for each scenario, we determine the probability of resolution as the percentage of realizations for which the patches are separated according to the above criterion. The probability of resolution is then averaged over all scenarios associated with a given patch distance. The resulting probabilites of resolution are listed in Table 3 for each distance and each of the examined source localization algorithms. Furthermore, Table 4 shows the corresponding DLE values. As can be expected, the probability of resolution generally increases with increasing patch distance while the DLE decreases. For distance 1, the patches are usually not resolved, but due to their proximity, the DLE values are smaller than for distance 2 or 3. With SISSY and a parameter $\alpha = 0.07$, the patches can be separated in almost all cases for distance 2 or higher. Furthermore, SISSY features higher probabilities of resolution and lower DLE values than STWV-DA and 4-ExSo-MUSIC, in particular for $\alpha = 0.07$. Even though the probability of resolution is sometimes better for cLORETA, the DLE values are considerably higher than for SISSY, which means that the overall source separation and localization for the considered scenarios is best when using SISSY with $\alpha = 0.07$.

probability of resolution (%)	distance 1	distance 2	distance 3	distance 4
cLORETA	56.0	100	96.7	95.0
STWV-DA	20.0	47.5	63.3	60.0
4-ExSo-MUSIC	8.0	35.0	93.3	100
L1-SISSY $\alpha = 0$	20.0	60.0	80.0	95.0
$L_{1,2}$-SISSY $\alpha = 0$	22.0	52.5	80.0	100
L1-SISSY $\alpha = 0.07$	28.0	95.0	100	100
$L_{1,2}$-SISSY $\alpha = 0.07$	34.0	97.5	96.7	100

Table 3: Average probability of resolution for each source localization algorithm and for four different patch distances.

3.4. Clinical data

In order to study the propagation phenomena that may potentially occur during the interictal spikes of the clinical data, we have systematically applied the tested source imaging algorithms to two time intervals corresponding to the first negative wave of the spike (time interval 1) and to the subsequent positive wave (time interval 2, cf. Fig. 10). For most patients, the source localization results were stable over both time intervals and we only observed a propagation of the epileptic spike for patient 1. Therefore, for patient 1, we show the results for both time intervals whereas for the other patients, we only display the results obtained for time interval 1.

For patient 1, source localization results obtained with the different algorithms are displayed in Fig. 10. cLORETA, STWV-DA, and 4-ExSo-MUSIC yielded very similar results for both time intervals, which is why, for these methods, we only show the solutions obtained for time interval 2. cLORETA

DLE (mm)	distance 1	distance 2	distance 3	distance 4
cLORETA	11.4	7.21	7.02	8.45
STWV-DA	20.4	20.4	18.5	18.4
4-ExSo-MUSIC	3.29	6.70	4.31	2.94
L1-SISSY $\alpha = 0$	2.56	5.21	4.42	3.28
$L_{1,2}$-SISSY $\alpha = 0$	3.30	5.57	4.85	2.69
L1-SISSY $\alpha = 0.07$	3.30	4.24	3.04	2.32
$L_{1,2}$-SISSY $\alpha = 0.07$	3.20	4.10	3.56	2.99

Table 4: Average DLE for each source localization algorithm and for four different patch distances.

shows high activation of the right temporal lobe and right occipital brain regions. STWV-DA and 4-ExSo-MUSIC identify approximately the same source region in the right temporal lobe. Concerning the identified active patches, the four tested variants of SISSY lead to comparable results, so we illustrate only the results of SISSY for $\alpha = 0$ and for $L_{1,2}$-SISSY for $\alpha = 0.07$. For time interval 1, SISSY identifies one region in the basal aspect of the right temporal pole, whereas for time interval 2, the estimated activation involves the posterior half of the right temporal lobe and the right temporo-occipital junction. According to the clinical interpretation of SEEG intracerebral data (cf. Figure 1), the brain regions involved in the interictal epileptic activity include the right basal temporal pole with posterior diffusion to the right middle temporal lobe. The source imaging results obtained by SISSY and the other tested source imaging algorithms are thus mostly concordant with the findings of the SEEG analysis. However, STWV-DA and 4-ExSo-MUSIC do not show the activation of the right temporal pole and cLORETA local-

izes also right occipital brain regions, which have not been observed to be involved in epileptic activity in the SEEG recordings. For both variants of SISSY, we also plot the estimated time signals within two seed patches comprising approximately 6 cm^2 of cortex and located on the temporal pole and in the posterior temporal cortex (see Fig. 10 bottom center). These two patches lie within the two brain regions identified by SISSY for the two considered time intervals. Fig. 10 bottom shows that the signal of the temporal pole is characterized by a high negative amplitude in the first time interval corresponding to the minimum of the epileptic spike. The patch in the posterior temporal lobe also has negative amplitude at the minimum of the spike, but the amplitude is much smaller than in the temporal pole, which explains why this activation is not visible in the thresholded SISSY solution for time interval 1. For time interval 2, the positive wave of the epileptic spike is slightly more pronounced in the posterior temporal lobe with a somewhat higher amplitude and longer duration. Comparing the signals estimated by the two variants of SISSY, it can be seen that for SISSY with $\alpha = 0$, the signals feature some small fluctuations and are not always the same for the dipoles within each patch. The signals extracted by $L_{1,2}$-SISSY are smoother and thus somewhat easier to interpret due to the exploitation of temporal structure in the algorithm.

For patients 2 to 4, we illustrate in Fig. 11 the source localization results obtained with SISSY for $\alpha = 0$ and $L_{1,2}$-SISSY for $\alpha = 0.07$ (both after AT) in comparison to the inverse solutions of cLORETA, STWV-DA, and 4-ExSo-MUSIC. For patient 2, SISSY and cLORETA localize the main activation at the minimum of the spike signal on the left temporal pole. $L_{1,2}$-SISSY for $\alpha =$

0.07 shows a very focal activation. cLORETA yields a similar solution, but the identified brain regions are slightly more posterior. STWV-DA localizes a brain region in the left insula. Finally, 4-ExSo-MUSIC identifies two patches: one in the left temporal pole and another one in the left insula. As reported in Figure 1, the regions involved in the intracerebral interictal activity include the left temporal pole, the insula and the mesial aspect of the left temporal lobe. The most concordant result is therefore obtained from 4-ExSo-MUSIC, but SISSY and the other tested algorithms are also able to retrieve part of the interictal network involved during SEEG recordings.

For patient 3, the two considered variants of SISSY lead to nearly identical results (see Fig. 11 middle), localizing a patch in the left superior precuneus. The maximal amplitudes estimated by cLORETA are also concentrated in this brain region, but in addition, cLORETA also shows an activation of the right superior precuneus and localizes several other small brain regions in occipital and temporal areas of the left hemisphere. STWV-DA identifies a large patch on the right superior precuneus. Finally, 4-ExSo-MUSIC identifies a number of small patches in the tissue remaining after the resection in the mesial and superior aspect of the occipito-parietal region. The SEEG recordings show that the epileptic spikes originate from the brain regions around the resected area and from the posterior cingulate gyrus. In particular the left mesial parieto-occipital brain regions and the left basal and superior precuneus (cf. Figure 1) are primarily involved in the interictal activity. For this patient, the source localization results of 4-ExSo-MUSIC are thus the most concordant with the SEEG analysis. The results of SISSY are less concordant, but remain in better agreement with intracerebral recordings

than those obtained by cLORETA. The results of STWV-DA do not match the observations made in the SEEG analysis.

In case of patient 4, both variants of SISSY localize a brain region on the right temporal pole, but this region is slightly smaller for $L_{1,2}$-SISSY with $\alpha = 0.07$. cLORETA identifies a large number of small brain regions scattered all over the right hemisphere, but involving in particular right mesial areas. STWV-DA and 4-ExSo-MUSIC both show an activation of the mesial part of the right temporal pole. According to the SEEG analysis, the brain region involved in epileptic spike activity corresponds to the anterior part of the right temporal lobe, mesially and laterally. This is concordant with the findings of SISSY, STWV-DA, and 4-ExSo-MUSIC, which retrieve either the mesial or the lateral aspect of the anterior temporal region, while the source localization result of cLORETA does not match the results from the intracerebral recordings.

4. Discussion

While the first algorithms that have been proposed for brain source localization over two decades ago are mainly suited for the identification of focal sources, over the past few years, researchers have paid increasing attention to the identification of spatially extended sources, which has been the topic of several previous studies (Limpiti et al., 2006; Friston et al., 2008; Ding, 2009; Bolstad et al., 2009; Birot et al., 2011; Chowdhury et al., 2013; Becker et al., 2014c; Zhu et al., 2014). The proposed algorithms are based on a variety of approaches, including extended source scanning, Bayesian, tensor-based, and sparse methods. When confronted with data of several simultaneously

active extended sources, the VB-SCCD algorithm has proved to be one of the most promising methods (Becker et al., 2014b, 2015), in particular in the case of correlated activities, and has been succesfully employed for the localization of brain regions involved in interictal epileptic spike signals (Zhu et al., 2013).

In this paper, we have strived to further improve the localization of extended sources by presenting a new regularized least squares algorithm called SISSY, which builds on the VB-SCCD method. As the VB-SCCD algorithm regularization only applies to the gradient of the source distribution, i.e., the variational map, which is invariant with respect to an added constant in the original source domain, it leaves an opening for source estimates that are amplitude-biased. This problem is successfully tackled by the additional L_1-norm regularization term employed by SISSY. However, as the single-patch simulation results show, the weight of this additional regularization term should be left small compared to the weight of the variational map regularization term because the quality of the source estimates declines with increasing influence of this term. This is somewhat surprising as one could have expected this sparsity-inducing term to help identify patches of small size. Yet the simulations have shown that besides avoiding the amplitude-bias, the new regularization term is only useful in the context of multiple patches, where it helps to separate close patches as demonstrated by the smaller DLE values for scenarios 2 to 4 and the higher probabilities of patch separation, but not for recovering single patches of small size. On the other hand, our observation that patches comprising less than 2.5 cm^2 of the cortical surface cannot be accurately identified (independently of the employed

regularization strategy) is corroborated by previous EEG and MEG studies, which have shown that a certain area of cortex (generally the minimum area is said to be 5 cm^2) needs to be active to obtain a signal of sufficient amplitude to be measurable at the surface (Mikuni et al., 1997; Oishi et al., 2002; Shigeto et al., 2002; Gavaret et al., 2006; Tao et al., 2005; Merlet and Gotman, 1999; Ebersole, 1997).

Following (Ou et al., 2009; Gramfort et al., 2012), we have also considered exploiting the temporal structure of the data by replacing the L_1-norm in the regularization terms by the $L_{1,2}$-norm. As the simulations show, this considerably improves the estimated time courses of the sources and leads to more robust source estimates, in particular in the case of several close patches, where it facilitates the patch separation.

Contrary to the method proposed in (Limpiti et al., 2006), 4-ExSo-MUSIC, and STWV-DA, SISSY is not based on a parameterization of the distributed source. This makes it more flexible with respect to the form of the patches as it can theoretically recover a patch of any form without preference for circular-shaped source regions like 4-ExSo-MUSIC or STWV-DA. Still, we have observed that SISSY also seems to have certain preferences for patch geometries, which cannot be characterized in general as they depend on the local characteristics of the cortical surface mesh.

A general problem with algorithms belonging to the family of regularized least squares approaches is the choice of the regularization parameter. Often this parameter is adjusted according to the noise level, which needs to be estimated from the measurements by analyzing a suitable data interval. In this paper, we have considered an alternative approach, where the reg-

ularization parameter is optimized with respect to the L_0-norm constraint, which maximizes the sparsity of the solution. This strategy works very well for single-patch scenarios. However, in the case of multiple patches, this approach tends to eliminate patches with weak amplitudes. The regularization parameter that is automatically selected using this method should thus be viewed as a maximum value, that gives a good indication of an adequate parameter. In practice, to avoid overlooking weaker sources, it is however advisable to check the source distributions obtained for somewhat smaller regularization parameters. Nevertheless, so far, our experience with the new regularization strategy on real EEG recordings is positive.

To delineate the source regions based on the source imaging solutions, the latter have to be thresholded. To this end, we have proposed to employ an AT method based on tools from image processing. To our knowledge, this is the first time that an AT method that is not based on a simple amplitude threshold is presented in the context of brain source imaging. The advantage of the proposed approach is that it is more objective than selecting a fixed threshold for the dipole amplitudes. As the AT approach segments the source distribution based on the gradient, it also permits to delineate source regions whose amplitude is only slightly larger than that of surrounding grid dipoles and which would have been very difficult to recognize using a fixed amplitude threshold. By contrast, this approach has some difficulties in adequately thresholding source distributions with very gradual amplitude changes because in this case, there is no significant change in gradient that can be exploited for the delineation of the sources. However, with an appropriate choice of the regularization parameter, this kind of source distribution

should not occur using SISSY.

For the simulations conducted in this paper, we use the same volume conductor and source space for the forward and the inverse problem, thereby neglecting the impact of modeling errors on the source localization results. However, the modeling errors would influence the results of all source localization algorithms such that their negligence does not give any advantage to the proposed method in particular. Nevertheless, the robustness to modeling errors of different source localization algorithms is an interesting subject that should be investigated in future studies.

To validate the proposed algorithm on clinical data, we have considered EEG recordings of four epileptic patients. In all cases, the brain regions identified by SISSY are concordant with the findings of an SEEG analysis, which was performed as part of the presurgical evaluation of these patients. Compared to the other tested methods, SISSY is more robust than STWV-DA and cLORETA, which sometimes lead to results that are less concordant with the SEEG analysis. Furthermore, SISSY is more precise in delineating the active brain regions than cLORETA. Finally, for one patient, the source localization results obtained by SISSY are more concordant with the findings of the SEEG analysis than those of 4-ExSo-MUSIC because SISSY accurately characterizes the propagation of the epileptic activity, which is not the case for 4-ExSo-MUSIC. On the other hand, 4-ExSo-MUSIC leads to slightly more concordant results with the SEEG for two other patients. For the last patient, SISSY and 4-ExSo-MUSIC perform equally well. For all patients, we do not observe big differences in the localized brain regions when considering the different variants of SISSY. However, on simulated

data, the performance improvement of $L_{1,2}$-SISSY with $\alpha = 0.07$ over SISSY with $\alpha = 0$ was only observed in the case of difficult scenarios with multiple patches, so the similarity of the results of these methods on the considered clinical data could be explained by the fact that the underlying source configurations are less complex. Finally, the exploitation of temporal structure based on the $L_{1,2}$-norm has also been shown to improve the interpretability of the estimated time signals in the case of clinical EEG data.

5. Conclusion

In conclusion, the computer simulations have shown that the SISSY algorithm proposed in this paper is better in separating multiple active patches than the other tested source imaging methods, provides an improved estimation of the source time signals by resorting to the $L_{1,2}$-norm regularization technique, permits to automatically delineate the active brain regions, and is computationally efficient. The clinical data examples have confirmed that SISSY yields results that are concordant with the expectations on the epileptic brain regions based on an SEEG analysis. Therefore, SISSY proves to be a promising method for the reconstruction of extended brain sources, in particular for application in epilepsy.

Future work will consist in extending the AT approach to other source imaging algorithms by making it more robust to different characteristics of estimated source distributions. Furthermore, we will apply the SISSY algorithm to more examples of clinical data in order to confirm the preliminary results of this paper. Another research direction will be the application of the SISSY algorithm for solving the electrocardiography inverse problem.

Acknowledgement

H. Becker was partly supported by Conseil Régional PACA and by CNRS France. The work of P. Comon was partly funded by the European Research Council under the EC 7th framework programme FP7/2007-2013 Grant Agreement no. 320594.

Alizadeh, F., Goldfarb, D., 2001. Second-order cone programming. Tech. Rep. 51-2001, Rutgers University.

Baillet, S., Mosher, J. C., Leahy, R. M., Nov. 2001. Electromagnetic brain mapping. IEEE Signal Processing Magazine 18 (6), 14–30.

Baldassarre, L., Mourao-Miranda, J., Pontil, M., 2012. Structured sparsity models for brain decoding from fmri data. In: Proc. of PRNI Conf. pp. 5–8.

Becker, H., Albera, L., Comon, P., Gribonval, R., Merlet, I., 2014a. Fast, variation-based methods for the analysis of extended brain sources. In: Proc. of EUSIPCO. Lisbon, Portugal.

Becker, H., Albera, L., Comon, P., Gribonval, R., Wendling, F., Merlet, I., 2014b. A performance study of various brain source imaging approaches. In: Proc. of ICASSP. Florence, Italy, pp. 5910–5914.

Becker, H., Albera, L., Comon, P., Gribonval, R., Wendling, F., Merlet, I., Nov. 2015. Brain source imaging: from sparse to tensor models. IEEE Signal Processing Magazine 32 (6), 100–112.

Becker, H., Albera, L., Comon, P., Haardt, M., Birot, G., Wendling, F., Gavaret, M., Bénar, C. G., Merlet, I., Aug. 2014c. EEG extended source localization: tensor-based vs. conventional methods. NeuroImage 96, 143–157.

Birot, G., Albera, L., Wendling, F., Merlet, I., 2011. Localisation of extended brain sources from EEG/MEG: the ExSo-MUSIC approach. NeuroImage 56, 102 – 113.

Bolstad, A., Van Veen, B., Nowak, R., 2009. Space-time event sparse penalization for magneto-/electroencephalography. NeuroImage 46, 1066 – 1081.

Boyd, S., Parikh, N., Chu, E., Peleato, B., Eckstein, J., 2010. Distributed optimization and statistical learning via alternating direction method of multipliers. Foundations and Trends in Machine Learning 3 (1), 1 – 122.

Boyd, S., Vandenberghe, L., 2004. Convex optimization. Cambridge University Press.

Chang, W., Nummenmaa, A., Hsieh, J., Lin, F., May 2010. Spatially sparse source cluster modeling by compressive neuromagnetic tomography. NeuroImage 53.

Chowdhury, R. A., Lina, J. M., Kobayashi, E., Grova, C., 2013. MEG source localization of spatially extended generators for epileptic activity: comparing entropic and hierarchical Bayesian approaches. PLOS ONE 8 (2), 1–9.

Combettes, P. L., Pesquet, J.-C., Dec. 2008. A proximal decomposition method for solving convex variational inverse problems. Inverse Problems (6).

Dale, A. M., Sereno, M. I., 1993. Improved localization of cortical activity by combining EEG and MEG with MRI cortical surface reconstruction: a linear approach. Journal of Cognitive Neuroscience 5 (2), 162–176.

Ding, L., 2009. Reconstructing cortical current density by exploring sparseness in the transform domain. Physics in Medicine and Biology 54, 2683 – 2697.

Ebersole, J. S., 1997. Magnetoencephalography/magnetic source imaging in the assessment of patients with epilepsy. Epilepsia 38, S1– 5.

Friston, K. J., Harrison, L., Daunizeau, J., Kiebel, S., Phillips, C., Trujillo-Barreto, N., Henson, R., Flandin, G., Mattout, J., 2008. Multiple sparse priors for the M/EEG inverse problem. NeuroImage 39 (1), 1104–1120.

Gabay, D., Mercier, B., 1976. A dual algorithm for the solution of nonlinear variational problems via finite elements approximations. Computers and Mathematics with Applications 2, 17–40.

Gavaret, M., Badier, J.-M., Marquis, P., McGonigal, A., Bartolomei, F., Regis, J., Chauvel, P., Aug. 2006. Electric source imaging in frontal lobe epilepsy. Journal of Clinical Neurophysiology 23 (4), 358–370.

Glowinski, R., Marrocco, A., 1975. Sur l'approximation, par éléments finis d'ordre un, et la résolution, par pénalisation-dualité, d'une classe de

problèmes de dirichlet non linéaires. Revue Française d'Automatique, Informatique, et Recherche Opérationelle 9, 41–76.

Gramfort, A., 2009. Mapping, timing and tracking cortical activations with MEG and EEG: Methods and application to human vision. Ph.D. thesis, Telecom ParisTech.

Gramfort, A., Kowalski, M., Hämäläinen, M., 2012. Mixed-norm estimates for the M/EEG inverse problem using accelerated gradient methods. Physics in Medicine and Biology 57, 1937 – 1961.

Gramfort, A., Papadopoulo, T., Olivi, E., Clerc, M., 2010. OpenMEEG: opensource software for quasi static bioelectromagnetics. BioMedical Engineering OnLine 45 (9).

Gramfort, A., Thirion, B., Varoquaux, G., 2013. Identifying predictive regions from fMRI with TV-ℓ_1 prior. In: Proc. of PRNI Conf.

Grech, R., Cassar, T., Muscat, J., Camilleri, K. P., Fabri, S. G., Zervakis, M., Xanthopoulos, P., Sakkalis, V., Vanrumste, B., Nov. 2008. Review on solving the inverse problem in EEG source analysis. Journal of NeuroEngineering and Rehabilitation 5.

Kybic, J., Clerc, M., Abboud, T., Faugeras, O., Keriven, R., Papadopoulo, T., 2005. A common formalism for the integral formulations of the forward EEG problem. IEEE Transactions on Medical Imaging 24 (1), 12 – 28.

Limpiti, T., Van Veen, B. D., Wakai, R. T., 2006. Cortical patch basis model for spatially extended neural activity. IEEE Transactions on Biomedical Engineering 53 (9), 1740 – 1754.

Ma, S., Yin, W., Zhang, Y., Chakraborty, A., 2008. An efficient algorithm for compressed mr imaging using total variation and wavelets. In: IEEE Proc. of CVPR. pp. 1–8.

Merlet, I., Gotman, J., Jun. 1999. Reliability of dipole models of epileptic spikes. Clinical Neurophysiology 110 (6), 1013 – 1028.

Mikuni, N., Nagamine, T., Ikeda, A., Terada, K., Taki, W., Kimura, J., Kikuchi, H., Shibasaki, H., 1997. Simultaneous recording of epileptiform discharges by MEG and subdural electrodes in temporal lobe epilepsy. NeuroImage 5, 298–306.

Moreau, J. J., 1962. Fonctions convexes duales et points proximaux dans un espace hilbertien. CR Acad. Sci. Paris Sér. A Math 255, 2897–2899.

Oishi, M., Otsubo, H., Kameyama, S., Morota, N., Masuda, H., Kitayama, M., Tanaka, R., 2002. Epileptic spikes: magnetoencephalography versus simultaneous electrocorticography. Epilepsia 43 (11), 1390–1395.

Ou, E., Hämäläinen, M., Golland, P., 2009. A distributed spatio-temporal EEG/MEG inverse solver. NeuroImage 44.

Pascual-Marqui, R. D., Michel, C. M., Lehmann, D., 1994. Low resolution electromagnetic tomography: A new method for localizing elecrical activity in the brain. Int. Journal of Psychophysiology 18, 49 – 65.

Shigeto, H., Morioka, T., Hisada, K., Nishio, S., Ishibashi, H., Kira, D., Tobimatsu, S., Kato, M., 2002. Feasibility and limitations of magnetoencephalographic detection of epileptic discharges: simultaneous recording

of magnetic fields and electrocorticography. Neurological Research 24 (6), 531–536.

Tao, J., Hawes-Ebersole, S., Ebersole, J., May 2005. Intracranial EEG substrates of scalp EEG interictal spikes. Epilepsia 46 (5), 669–676.

Tibshirani, R., Saunders, N., 2005. Sparsity and smoothness via the fused LASSO. Journal of the Royal Statistical Society B 67 (Part I), 91 – 108.

Vincent, L., Soille, P., Jun. 1991. Watersheds in digital spaces: an efficient algorithm based on immersion simulations. IEEE Transactions on Pattern Analysis and Machine Intelligence 13 (6), 583–598.

Wagner, M., Fuchs, M., Wischmann, H. A., Drenckhahn, R., 1996. Smooth reconstruction of cortical sources from EEG and MEG recordings. NeuroImage 3 (3), S168.

Wipf, D., Nagarajan, S., 2009. A unified Bayesian framework for MEG/EEG source imaging. NeuroImage 44, 947 – 966.

Yao, J., Dewald, J. P. A., Apr. 2005. Evaluation of different cortical source localization methods using simulated and experimental EEG data. NeuroImage 25 (2), 369–382.

Zhu, M., Zhang, W., Dickens, D. L., Ding, L., 2014. Reconstructing spatially extended brain sources via enforcing multiple transform sparseness. NeuroImage 86, 280–293.

Zhu, M., Zhang, W., Dickens, D. L., King, J. A., Ding, L., 2013. Sparse MEG

source imaging for reconstructing dynamic epileptic sources of interictal spikes. Journal of Clinical Neurophysiology 30 (4), 313–328.

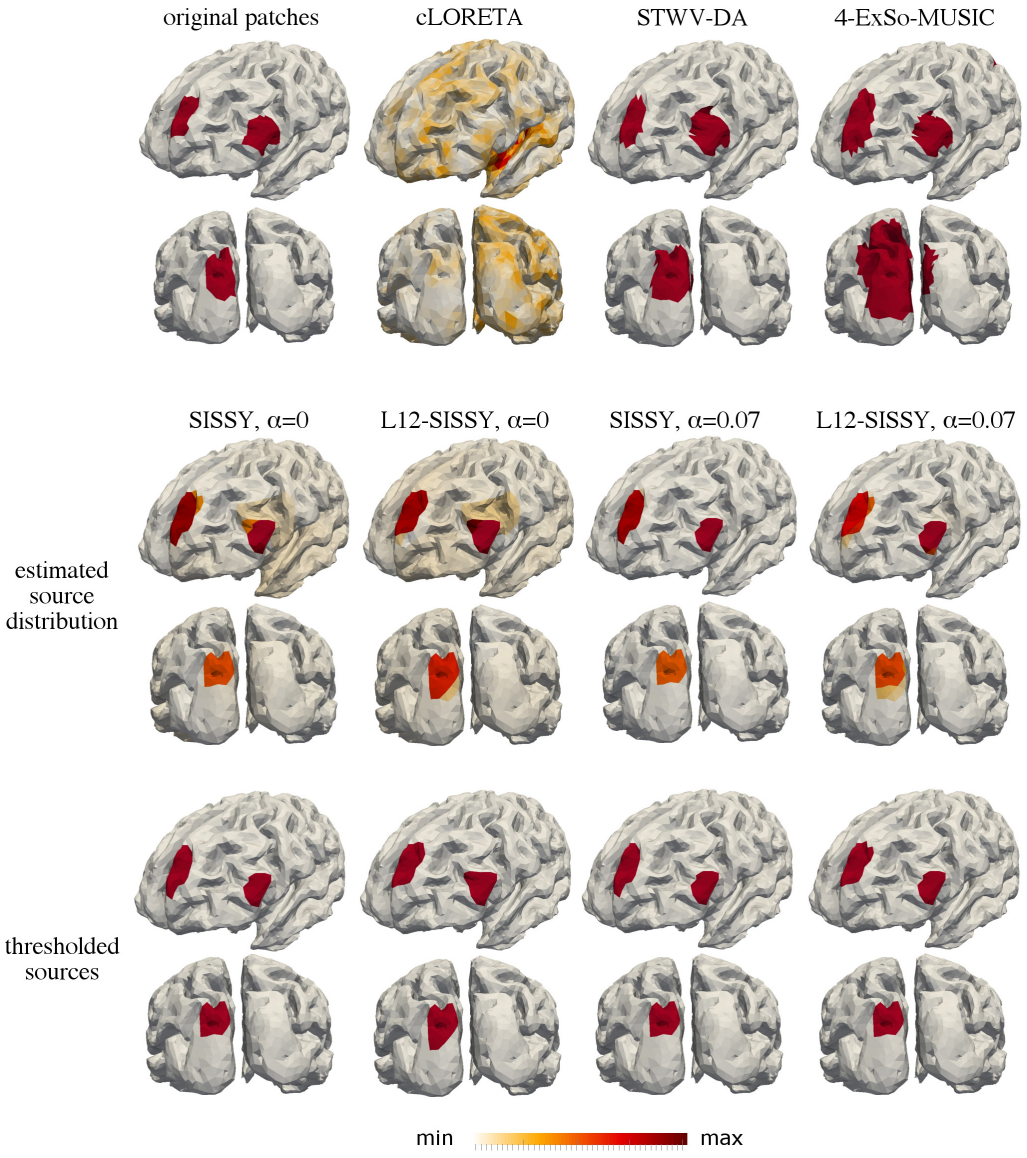

Figure 5: Patches SupFr, InfFr, and SupOcc (scenario 1), inverse solutions of cLORETA, STWV-DA, and 4-ExSo-MUSIC and estimated source distributions and thresholded sources for four variants of SISSY.

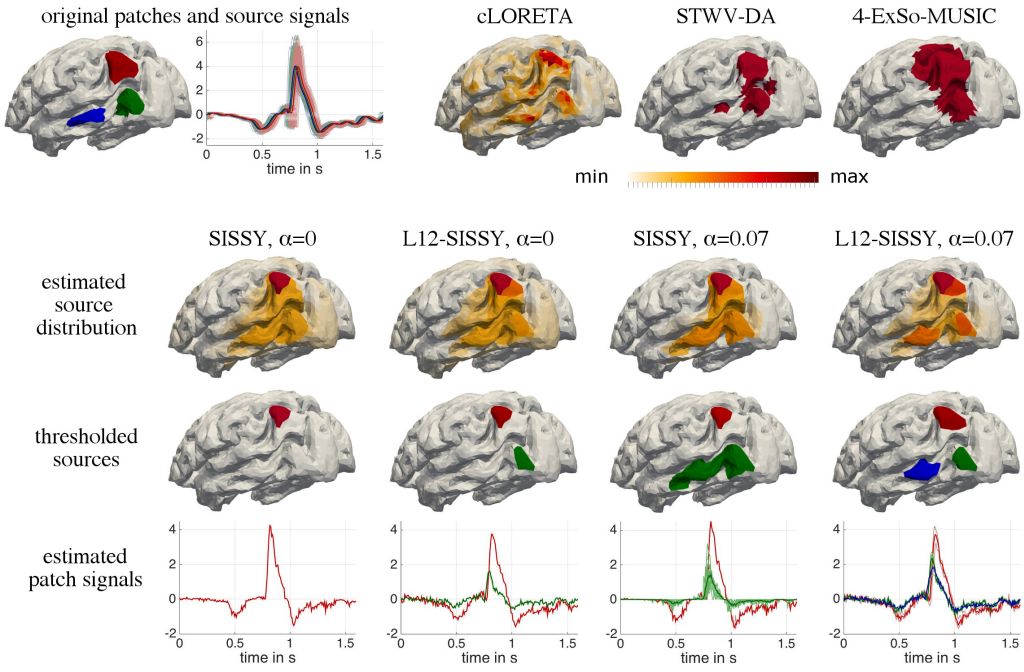

Figure 6: Patches MidTe, OccTe, and InfPa (scenario 2), inverse solutions of cLORETA, STWV-DA, and 4-ExSo-MUSIC and estimated source distributions and thresholded sources for four variants of SISSY.

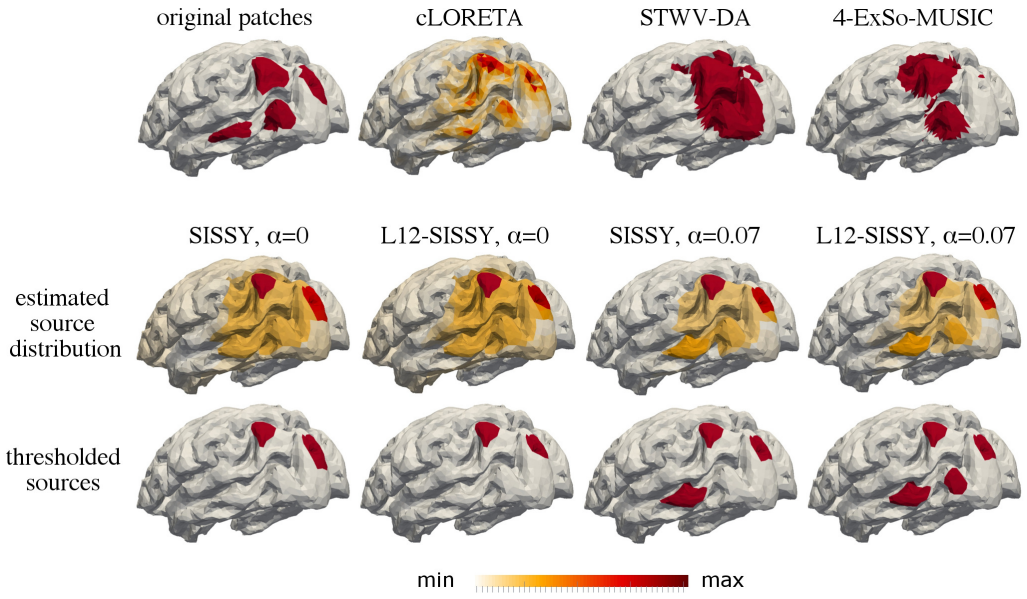

Figure 7: Patches OccTe, MidTe, SupOcc, and InfPa (scenario 3), inverse solutions of cLORETA, STWV-DA, and 4-ExSo-MUSIC and estimated source distributions and thresholded sources for four variants of SISSY.

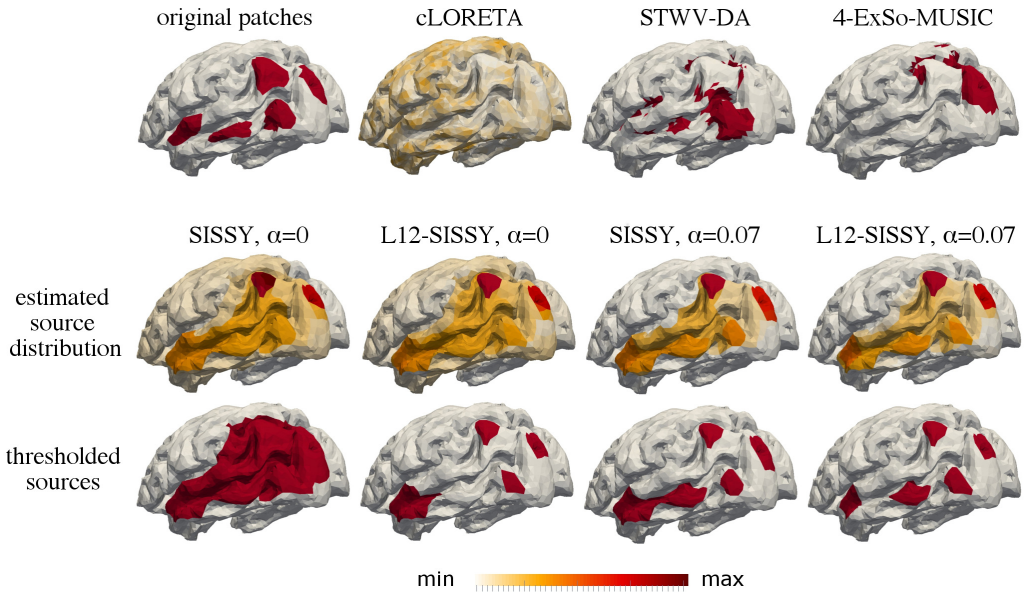

Figure 8: Patches OccTe, MidTe, InfPa, SupTe, and SupOcc (scenario 4), inverse solutions of cLORETA, STWV-DA, and 4-ExSo-MUSIC and estimated source distributions and thresholded sources for four variants of SISSY.

Figure 9: Six patches considered for the analysis of patch separation.

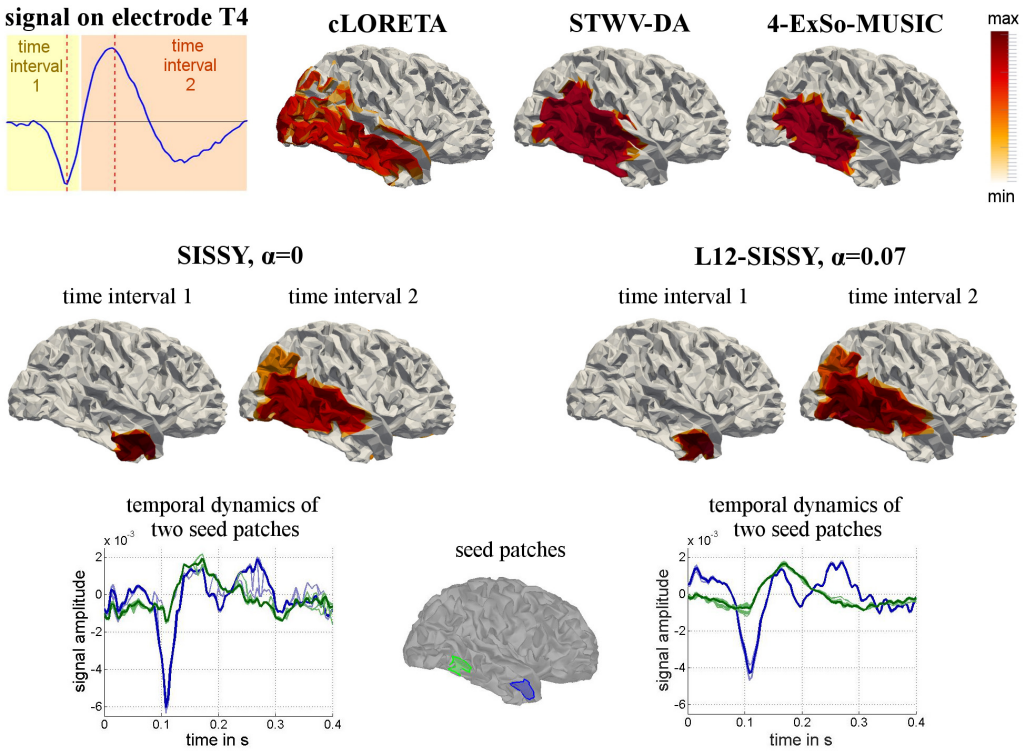

Figure 10: Clinical data of patient 1: Source localization obtained for epileptic spikes maximal on electrode T4. The two considered time intervals (corresponding to the first and second part of the spike) are marked in yellow and orange. The time points (one within each interval) for which the source localization results are displayed are marked by red dotted lines and correspond to the minimum and the maximum of the epileptic spike. For cLORETA, STWV-DA, and 4-ExSo-MUSIC, we display only the results obtained for time interval 2 (results for time interval 1 are comparable). For SISSY, the amplitudes of the brain regions inactive according to AT have been set to 0 and for cLORETA, the amplitudes of the brain regions not selected by the GOF have been set to 0. For SISSY, we also display the estimated source dynamics within two seed patches located within the regions localized during the first and second time interval. Pale blue and pale green signals show dynamics of individual dipoles within each patch whereas dark blue and dark green signals correspond to the average signals of each patch.

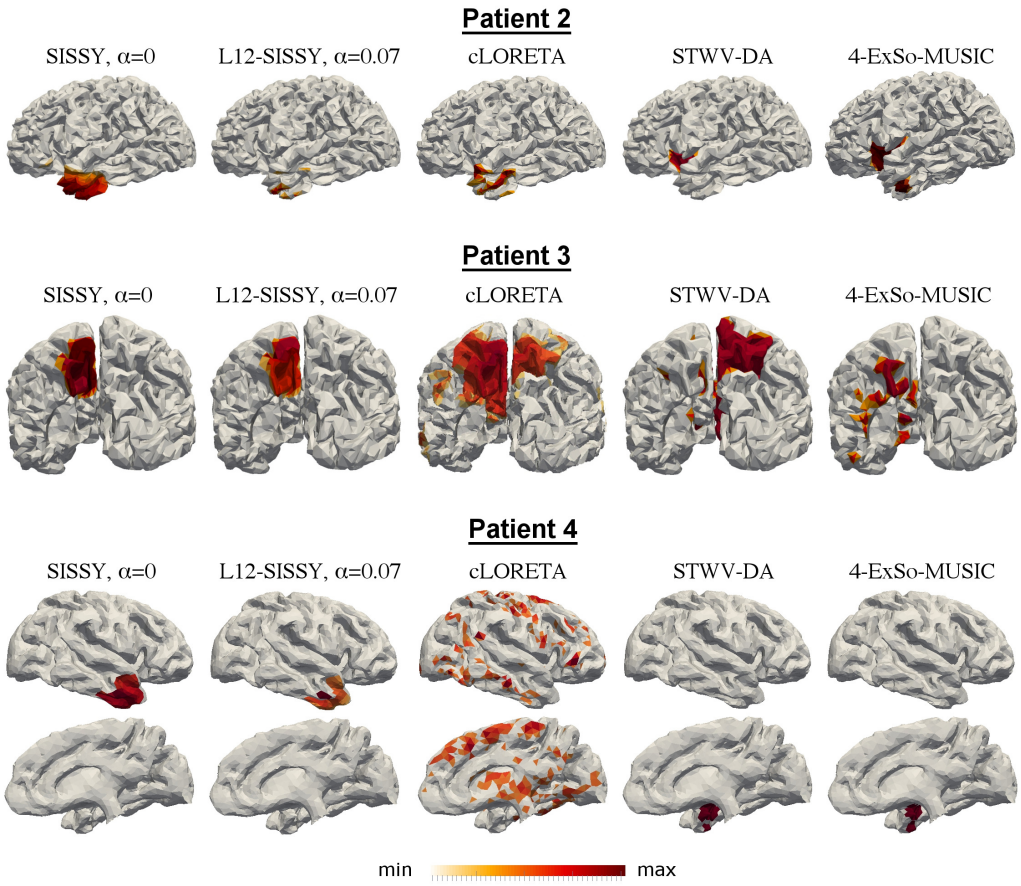

Figure 11: Clinical data of patients 2 to 4: Source localization obtained for epileptic spikes maximal on electrode FFT9 for patient 2, on electrode PPOz for patient 3, and on electrode FT10 for patient 4. For SISSY, the amplitudes of the brain regions inactive according to AT have been set to 0 and for cLORETA, the amplitudes of the brain regions not selected by the GOF have been set to 0.